

Microstructural Influence on Thermoelectric Properties of CaMnO₃ Ceramics

Samanta de O. A. Torres^a , Daniel Thomazini^{a*} , Gabriel P. Balthazar^a, Maria V. Gelfuso^a 

^aUniversidade Federal de Itajubá (UNIFEI), Grupo de Desenvolvimento de Materiais Funcionais (GDMaF), Av. BPS, 1303, Bairro Pinheirinho, Itajubá, MG, Brasil

Received: April 23, 2020; Revised: July 28, 2020; Accepted: August 28, 2020

Thermoelectric properties of pure polycrystalline CaMnO₃ ceramics were significantly enhanced by increasing sintering holding time from 1 to 24 h. The Seebeck coefficient values were reduced while the sintering holding time was increased, and the DC electrical conductivity was enhanced from 255 S/m to 1.748 S/m. This same effect was observed in electronic thermal conductivity, increasing from 5×10^{-3} to 3.5×10^{-2} W/m K, whereas the lattice thermal conductivity decreased from 5.0 to 4.0 W/m K at 873K. Overall, CaMnO₃ ceramic sintered for 24 h demonstrated the best performance, which presented a Figure-of-Merit value of about 0.03. The grain size of the samples ranged from 2.79 μ m to 6.45 μ m, due to the sintering holding time, directly influencing the high-temperature thermoelectric properties of CaMnO₃ ceramics.

Keywords: Calcium manganite, thermoelectric, sintering time.

1. Introduction

The environmental impacts caused by fossil fuels are quite significant and, also, one of the main sources of residual heat comes from cars, as approximately 60% of the fuel energy is lost as heat¹. Some of this wasted energy can be harvested and converted directly into electrical energy, enhancing the efficiency of electrical devices, like hybrid vehicles. Thermoelectric materials appear as an alternative to convert thermal energy directly into electrical energy from a temperature gradient, which induces a flux of charge carriers from the hottest to the coldest region in the material. The efficiency of the thermoelectric conversion is evaluated using the Figure of Merit (*ZT*) values, which is calculated from the Equation 1, as follows²:

$$ZT = (S^2 \sigma / \kappa) T \quad (1)$$

High *ZT* values are obtained if thermoelectric materials exhibit low thermal conductivity (κ) and high values of Seebeck coefficient (*S*) and electrical conductivity (σ). Intermetallic materials, such as alloys based on tellurides and silicon-germanium, have *ZT* values higher than unity^{1,3}, but these materials have limitations because they do not support oxidative environments. On the other hand, although thermoelectric oxides do not present satisfactory values of *ZT*, they are a viable option for acting as thermoelectric materials due to their stability at high temperatures and oxidant environments⁴. The most promising p-type oxides are compounds based on cobaltites of alkaline or alkaline earth metals, such as Ca₃Co₄O₉⁵ and Na_xCoO₂ having values of *ZT* up to 0.27⁶ and 0.72⁷ at 600 °C, respectively.

Perovskite oxides like CaMnO₃ (CMO) and SrTiO₃ ceramics are well-advised as most promising n-type thermoelectric ceramics, due to the flexibility respect to doping at both sites⁴,

A and B. Also, these oxides exhibit high thermal conductivity that causes a drop in the *ZT* values⁸. Its advantages are due to the values of its thermoelectric properties, that is, high values of Seebeck coefficient ($|S|_{300K} > 400 \mu\text{VK}^{-1}$)⁹ and reasonable values of electrical conductivity ($\sigma_{873K} \geq 700 \text{ S/m}$)^{10,11}. Studies carried out on this oxide, involve the modification of several parameters, which include doping, differentiated methods of synthesis, calcination and sintering atmospheres, seeking to understand how these parameters alter the thermoelectric properties of the material^{8,12-14}. Studies about CMO presented in literature get *ZT* values in the range 0.018-0.075^{11,15,16} and SrTiO₃ presented values of 0.01 at 500 °C¹⁷. Furthermore, to obtain a good thermoelectric device, the *ZT* values must be close between the type-n and type-p materials¹⁸. The n-type oxides still need to be further studied because they do not have *ZT* values as good as p-types materials.

Calcium Manganite, or CMO, is a perovskite ceramic with an orthorhombic crystalline structure, and n-type semiconductor characteristics, which has been the object of several studies¹⁹⁻²² to improve its thermoelectric parameters. The synthesis process can improve the thermoelectric properties of the material. Bocher et al.⁸ and Lan et al.²³ studied the synthesis of CMO based ceramics using two different routes. They reported that *ZT* values obtained by chemical route were higher than the ones achieved by solid-state reaction, mainly due to the difference in grain size obtained for each route. Some studies demonstrate that large grain sizes provide improvements in the values of electrical conductivity²⁴⁻²⁶. Thus, one of the ways not widely explored by research would be to produce ceramics with larger grains by increasing the sintering time, intending to increase the *ZT* values.

This study aims to reports the effects of sintering holding time on the grain size, structure, microstructure, and the thermoelectric properties of CaMnO₃ ceramics prepared by solid-state reaction method.

*e-mail: thomazini@unifei.edu.br

2. Experimental Procedure

Raw precursors CaCO_3 (Impex, 99.0%) and MnO (Sigma-Aldrich, 99.0%) were mixed in ball mill for 3.5 h into polypropylene jar containing deionized water (DIW) obtained by process of reverse osmosis (RO), presenting electrical conductivity of 0.05 S/m, and zirconia grinding media. The dried powder was calcined at 1273 K, as suggested by thermogravimetric (TG) and differential thermogravimetric (DTG) analyses (Netzsch STA-449). The structural analysis of the calcined powders was performed by X-Ray Diffraction (XRD)(Bruker D8 ADVANCE) using $\text{CuK}\alpha$ radiation. Microstructural observations were evaluated by a Scanning Electron Microscopy (SEM) with a PHENOM Pro-X, aided by the Energy Dispersive Spectroscopy (EDS) for semiquantitative analysis of chemical elements.

After calcination, the samples were uniaxially pressed at 160 MPa into discs and presented a thickness and diameter of 1.5 mm and 12 mm, respectively. After, dilatometric analysis (Netzsch DIL 402PC) was performed to determine the ideal sintering temperature. The samples were sintered at 1498 K in a tubular resistive furnace with different sintering times of 1, 3, 6, 12 and 24 h with airflow by natural convection. After sintering, XRD analyses were performed to assess crystalline phases present in the ceramics. SEM was conducted to observe the morphology and aided to measure the particles and the grain size of the samples.

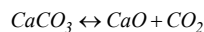
The lattice parameters were obtained from the structural refinement using the Rietveld method, thus, the theoretical density for each sample was obtained. The apparent densities of the ceramics were determined by the Archimedes method. The average particle and grain size were measured using the ImageJ software²⁷.

The electrical conductivity values were obtained using the 4-probe DC method. The measurement of the Seebeck coefficient was performed using a ΔT of 10 K. These two measurements (WT Industria-SB01) were conducted from room temperature up to 873 K in the air atmosphere. The thermal diffusivity (α) measurements (Netzsch LFA-427) were carried out from room temperature up to 873 K in the

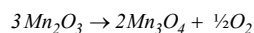
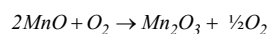
N_2 atmosphere at 50 mL/min, using the pulsed laser technique. From α values, the thermal conductivity was calculated using the equation $\kappa(T) = C_p(T) \cdot \delta(T) \cdot \alpha(T)$, where, C_p is the specific heat and δ is the theoretical density. Following the ZT equation (Equation 1), the Figure of Merit values were calculated using the data obtained from the previous measurements, referring to the thermoelectric parameters.

3. Results and Discussions

Figure 1 presents the TG and DTG curves for the mixture of the precursors for CMO composition, as well as the curves of each precursor. TG curve to CaCO_3 shows mass loss regarding the thermal decomposition of CaCO_3 to CaO , as follows²⁸:



At the TG/DTG MnO curves there is a mass gain of approximately 12% (expected value = 11.3%) in the interval of 300 K to 1173 K due to oxidation of MnO to Mn_2O_3 in air atmosphere. Close to 1173 K, beholds a mass loss related to the manganese oxide reduction from Mn_2O_3 to Mn_3O_4 , and at 1203 K, without mass variation, it is noticed a phase transition. These events occur following the reactions below^{29,30}:



From the TG curves, it is possible to observe that the chemical reactions to form the CMO phase are completed around 1273 K, so, this temperature was adopted for the calcination of the powder. Mouyane et al.³¹ also observed that after 1273 K there is no more occurrence of any reaction in CMO powder.

Based on dilatometric analysis for green CMO ceramic, the sintering temperature was set at 1498 K. Some studies have announced sintering temperature at 1423 K³², 1473 K²⁰, 1573 K³³, 1623 K¹², indicating that this adopted sintering temperature is in accordance with the literature.

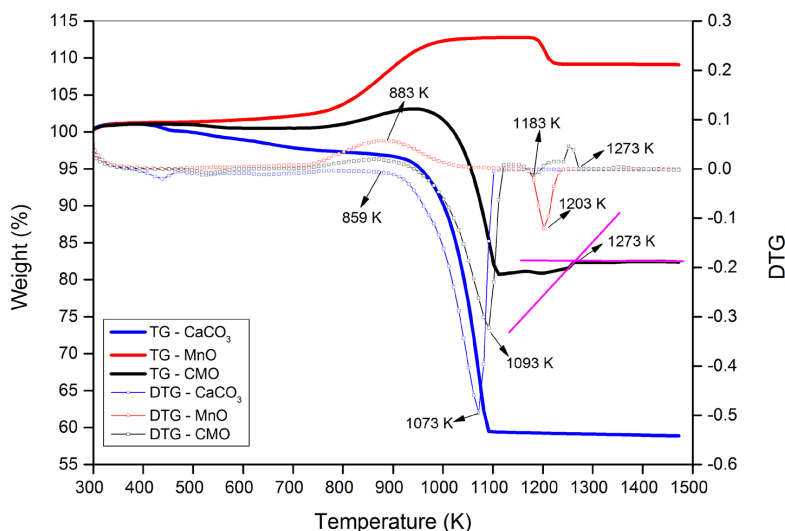


Figure 1. TG/DTG curves for raw precursors and CMO mixture.

The XRD patterns for calcined powder and sintered ceramics are presented in Figure 2. From XRD characterization, theoretical density about 4.58 g/cm³ was obtained for CMO powder. The CMO phase major peaks have been indexed in the orthorhombic system, as shown in Figure 2a, but also, it can be perceived the presence of a small amount of marokite (CaMn₂O₄) as a secondary phase. From the XRD pattern of the sintered ceramics (Figure 2b, c, d, e, and f), it can be observed the exclusive presence of CaMnO₃ single-phase. Some studies^{34,35} attribute the appearance of this secondary phase to the low calcination temperature. The higher sintering temperature can be responsible for avoiding the permanence of the CaMn₂O₄ phase, favoring the consolidation of the exclusive CaMnO₃ phase in the ceramics. Due to CMO be one of the stoichiometric phases in the CaO-MnO phase diagram, a small deviation in the Ca/Mn concentration ratio can promote the formation of marokite, which can induce mechanical stress inside of the material and produce

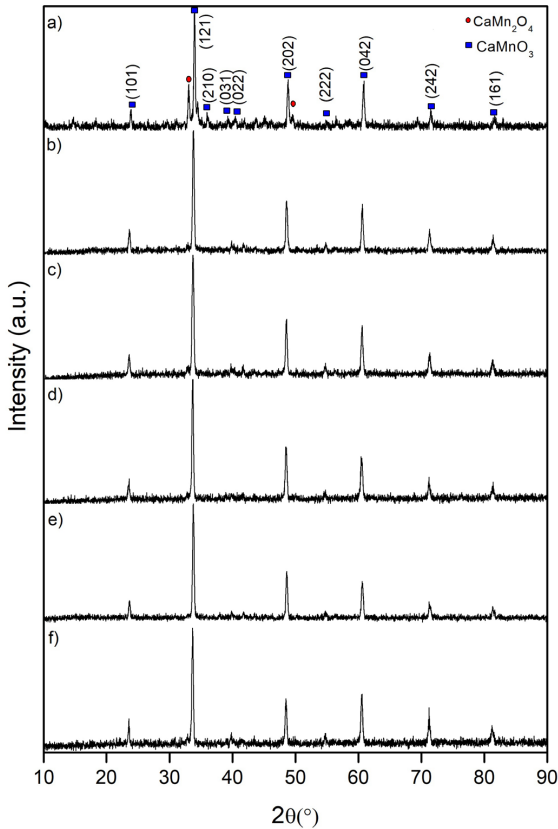


Figure 2. XRD patterns of the samples: a) powder, b) CMO-1h, c) CMO-3h, d) CMO-6h, e) CMO-12h and f) CMO-24h.

microcracks. However, this effect can be avoided when the reaction of the precursors occurs at higher temperatures³⁶⁻³⁸.

Table 1 presents the values of lattice parameters and unit cell volume (*V*) for ceramics sintered at different holding times. It can be noted the value of $207.96 \pm 0.10 \text{ \AA}^3$ as the largest cell volume calculated to CMO ceramic sintered for 1 h (CMO-1h), $207.65 \pm 0.12 \text{ \AA}^3$ was obtained to CMO-12h while 207.44 ± 0.06 was computed to CMO-24h. It has been reported that CMO ceramics with high concentration of Mn³⁺ cation in the lattice is due to oxygen loss³⁹, which depends on the processing method used to produce the ceramics, since the oxygen vacancy content affects the Mn³⁺/Mn⁴⁺ ratio⁴⁰. However, no significant variation was observed in cell volume for CMO-1h, CMO-3h, CMO-6h, CMO-12h. A very slightly decrease in cell volume is noted for CMO-24h, suggesting that the Mn³⁺/Mn⁴⁺ ratio content was affected by long sintering holding time. Fu et al.⁴¹ reported in their work that the variation in the sintering time causes changes in the lattice parameters and decreases the concentration of Mn⁴⁺. Wang et al.⁴², attributed the decrease in unit cell volume to Mn-O-Mn (*d*_{Mn-O-Mn}) linkage distance reduction, which may enhance the Mn-O bond. Structural distortions are associated with this behavior and suggest the correlation between crystal structure and electrical transport properties. Thus, CMO-24h ceramic should present the shortest *d*_{Mn-O} bond. So, the overlap between Mn3*d* and O2*p* orbitals of the system is expected. Thus, the electron hopping between Mn³⁺ and Mn⁴⁺ is facilitated by interactions between these orbitals, which will influence strongly the electrical conductivity. This argument will be considered in posterior discussion about thermoelectric discussion.

The relative densities, apparent porosity and grain size of the ceramics are listed in Table 2. It is noted the increase in the densification and the decreasing of apparent porosity with sintering time, so, the ceramic with the highest relative density value is the CMO-24h. According to Mazur³⁶, rising the sintering temperature, the CMO ceramics undergo the increasing of densification and porosity stabilization. Nevertheless, the evaluation of the sintering time is not usually studied due to huge different synthesis and sintering conditions. The increase of the sintering time rises the densification of the samples and of the grain size, thus, decreasing the porosity. This occurs due to the enhancement of the diffusion process, which leads to an increase the grain size, and consequently, decreasing the surface energy in the grain boundary^{43,44}.

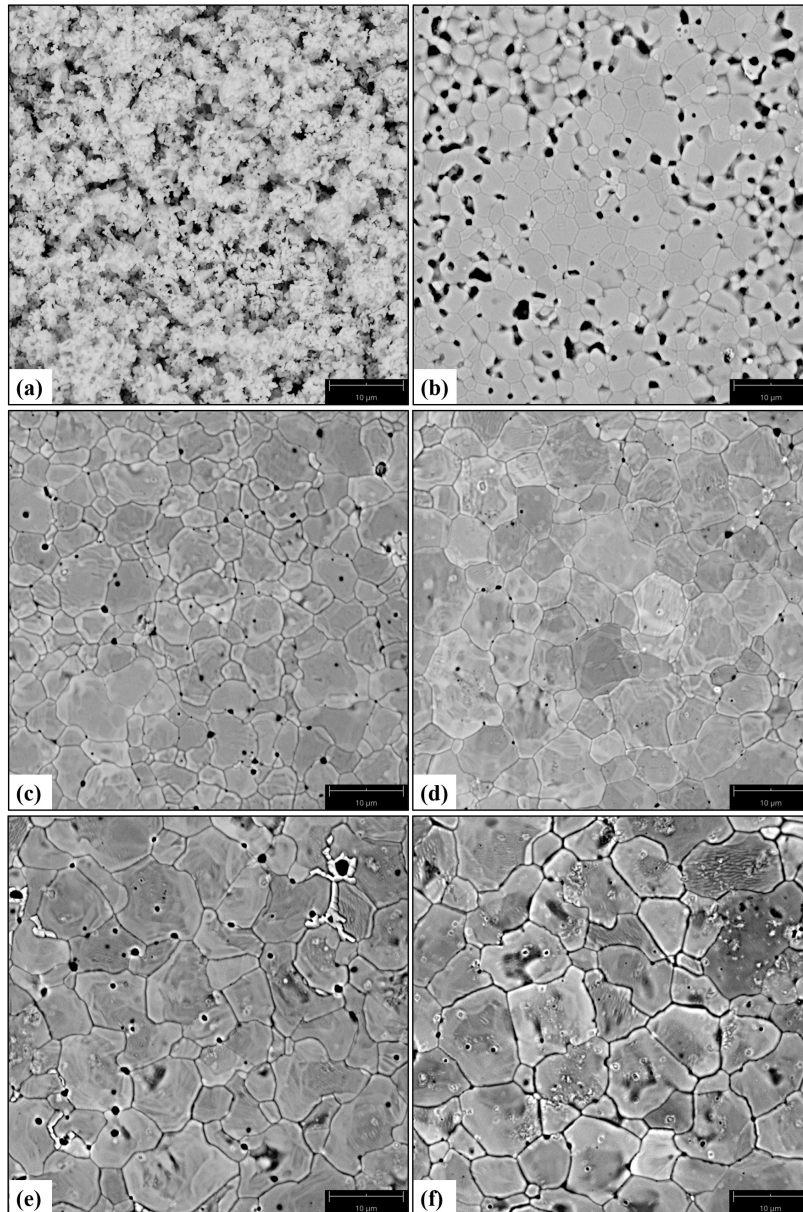
Figure 3 shows the SEM images for the powder (Figure 3a) and for the sintered ceramics (Figure 3b to 3f). It is clear that the average grain size of the CMO ceramics increases with the increase of the holding time.

Table 1. Lattice parameters and cell volume for CMO ceramics sintered at different holding times.

Sample	Lattice parameters (Å)			V (Å ³)
	a	b	c	
CMO-1h	5.280 ± 0.001	7.473 ± 0.002	5.271 ± 0.002	207.96 ± 0.10
CMO-3h	5.280 ± 0.001	7.468 ± 0.002	5.266 ± 0.001	207.63 ± 0.08
CMO-6h	5.272 ± 0.001	7.451 ± 0.002	5.286 ± 0.001	207.67 ± 0.08
CMO-12h	5.268 ± 0.002	7.461 ± 0.003	5.283 ± 0.001	207.65 ± 0.12
CMO-24h	5.275 ± 0.001	7.468 ± 0.001	5.265 ± 0.001	207.44 ± 0.06

Table 2. Relative density, apparent porosity and grain size for CMO ceramics sintered with different holding time.

Sample	CMO-1h	CMO-3h	CMO-6h	CMO-12h	CMO-24h
Relative Density (%)	83.3	88.2	96.9	97.5	99.4
Apparent Porosity (%)	15.5	1.7	2.9	0.7	0.8
Grain Size (μm)	2.79 ± 0.79	3.03 ± 1.04	3.78 ± 1.40	5.41 ± 2.43	6.45 ± 3.06

**Figure 3.** SEM images of the a) powder, b) CMO-1h, c) CMO-3h, d) CMO-6h, e) CMO-12h and f) CMO-24h ceramics.

The average grain size measured from SEM images is listed in Table 2. Also, it is possible to note the increase of the grain size dispersion due to the uneven grain growth. These changes in morphology are mainly caused by high calcination temperatures and long sintering times^{40,45}. SEM images for ceramics with 6, 12 and 24 h of sintering time, Figure 3d, 3e and 3f, respectively, shows that the microstructures are in good agreement with the dense materials and consequently small porosity.

The grain size obtained for CMO ceramics in other studies ranged between 3 and 5 μm for sintering temperature of 1473 K for 10 hours¹⁰, 1573 K for 24 hours and 1623 K for 36 hours⁴⁶. In the present study, the densities of the ceramics were between 83.3% and 99.4%, while in others studies these values were between 76% for sintering temperature of 1473 K for 10 hours³⁷ and 97.8% for sintering temperature of 1573 K for 12 hours⁴⁷.

In the conductive or semiconductor materials, the contribution of electronic charge carriers in the thermal conductivity (κ_e) is described by Wiedemann-Franz Law⁴⁸ (Equation 2):

$$\kappa_e = \sigma LT \quad (2)$$

Where σ is the electrical conductivity, L is the Lorenz constant and T is the absolute temperature. The curves in Figure 4 indicate that κ_e values increase with temperature. Furthermore, the contribution of κ_e for thermal conductivity does not exceed 0.50% of total κ , indicating that the most significant contribution is related to the lattice (κ_l) thermal conductivity. In agreement with other studies, the contribution of an electronic component (κ_e) in comparison to the lattice component (κ_l) could be negligible^{19,37,46,49}, behavior expected for materials with low electrical conductivity, as insulator and semiconductor materials. It is noted the decrease of κ_l values as temperature increases, which is characteristic of the insulating ceramics. Moreover, longer sintering time promoted an increase in the thermal conductivity values

of the ceramics⁵⁰. The presence of pores can decrease the thermal conductivity values because air has lower values than all the ceramics (0.026 W/m K)⁵¹. Thermal conduction by phonons is the main heat mechanism transport in ceramics. Thus, the process of phonon spreading caused by the presence of pores and grain boundary is responsible for the decrease in the mean free path of phonons, which causes a decrease in the thermal conductivity values^{50,52}. The decreasing in lattice thermal conductivity with increasing temperature can be explained by the increase in the number of phonons that participate in the phenomenon of heat transport and, consequently, the increase of the probability of these collide and/or interact which results in an “Umklapp process”, that reduces the heat transfer efficiency of phonons and therefore reduces the thermal conductivity as the temperature rises. The thermal conductivity is strongly influenced by the density of the ceramics, so the densest samples have the highest values of thermal conductivity and vice-versa⁵³.

The electrical conductivity values (σ) of the CMO ceramics are shown in Figure 5. As noticed in Figure 5a,

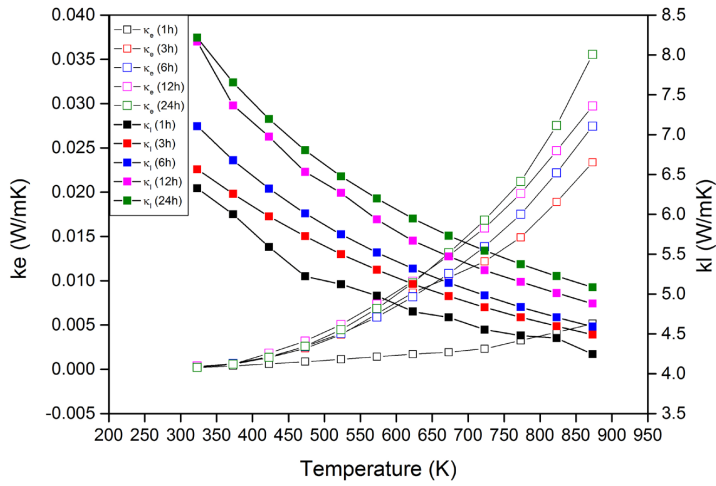


Figure 4. Electronic and lattice components of the thermal conductivity for the CMO ceramics.

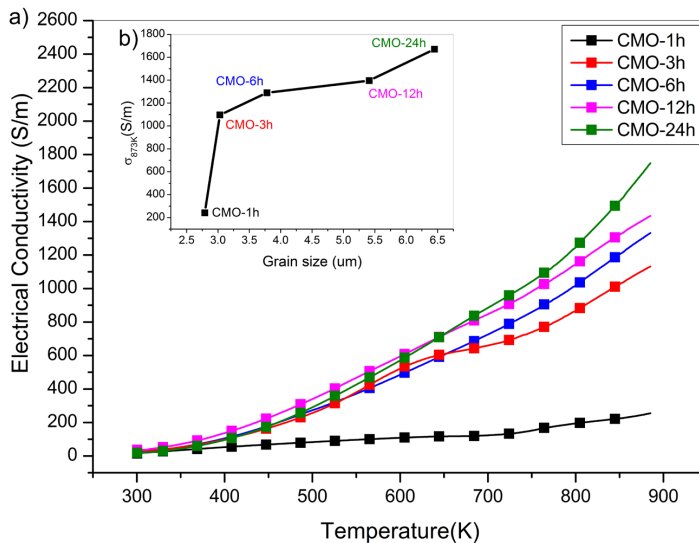


Figure 5. a) Temperature and b) grain size dependence of electrical conductivity for CMO ceramics.

σ values increases with temperature for all ceramics, and the highest value (1748 S/m) was obtained for CMO-24h at 873 K. Also, the σ -T curves for all the specimens are similar up to 650 K. Yang et al.⁴² reports that manganese perovskites based ceramics present the mechanism of electrical conduction of small polaron, explained by Mott-Davis equation⁵⁴, given by the Equation 3.

$$\sigma = \frac{C}{T} \exp\left(-\frac{E_a}{K_B T}\right) \quad (3)$$

Where C is a pre-exponential factor referring to intrinsic characteristics of the crystalline lattice of material and provide information related to the carrier scattering mechanism⁵⁵, T is the absolute temperature, E_a is the activation energy for hopping conduction mechanism and K_B is the Boltzmann constant. The increase of the temperature is responsible for assist the electron hopping through the small polaron mechanism^{56,57}. The electrical conductivity values diverge in literature, due to different synthesis methods and sintering conditions of the ceramics^{10,37,47}. These different synthesis and sintering methods strongly affects the number of defects, such as grain boundaries⁵⁸, which directly influence the mobility of carriers. The relation between grain size and electrical conductivity of the ceramics at 873K is presented in Figure 5b. As the grain size increases, due to effect of sintering time, the electrical conductivity values rise. High grain size values imply into the reduction of grain boundaries, thus the scattering centers are reduced, consequently, the electrical conductivity increases^{26,59,60}. The electrical conductivity values obtained in the literature range between 500 S/m⁴⁹ and 700 S/m¹⁰, for ceramics produced by solid-state reaction or chemical method⁹, calcined at 1373 K, and sintering temperature between 1473K and 1523K.

Based on Equation 3, the activation energy calculated for CMO ceramics are presented in Table 3.

The activation energy values obtained by other authors for CMO ceramics varied between 0.08⁶¹ and 0.38 eV⁶², thus, the values obtained in the present study are in agreement with other studies. The difference perceived to other values achieved in literature, based on Equation 3, occurred due to the impurities and the crystallinity of the sample^{13,49}. However, in the present study, it is noticed about the same E_a values for CMO-3h to CMO-24h ceramics, indicating in this case, the sintering time does not significantly affect the E_a values³³. The slight difference in band gap energy for CMO-1h compared to other ceramics can be induced by structural distortions, gives rise to the different resistivities of the samples, even though they have almost equal electron carrier concentration⁴². These distortions could be related to higher amount of grain boundary in this ceramic, presenting higher electrical resistivity, as previous discussed.

Figure 6 shows the temperature dependence of the Seebeck coefficient (S) values. The values of the Seebeck coefficient depends strictly on the electronic structure of the material^{34,46}. The negative value of S is characteristic of n-type material, in which the electrons are the major charge carriers. When the material is submitted to a gradient temperature, it presents a higher concentration of electrons on the hot side, creating an opposite electrical voltage with temperature gradient^{20,47,63}. The modulus of Seebeck coefficient values decreases with the increasing temperature, which may explain the behavior of the semiconductor material due to an increase in the concentration of the carriers with the temperature^{12,64}. For the temperatures above 600 K occurs the stabilization effect, in which the Seebeck coefficient is not dependent on the temperature. The Seebeck coefficient can be given

Table 3. Activation energy for CMO ceramics sintered at different holding times.

Sample	Activation energy (eV)				
	1h	3h	6h	12h	24h
CMO	0.13	0.20	0.19	0.19	0.22

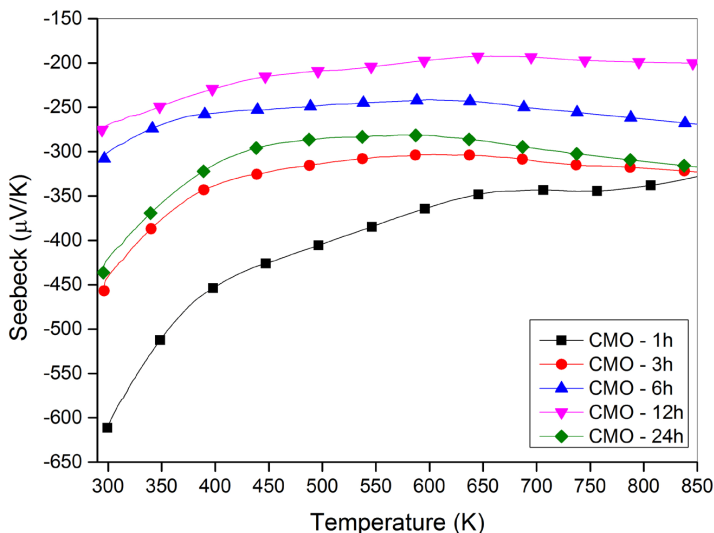


Figure 6. Seebeck coefficient values for the CMO ceramics.

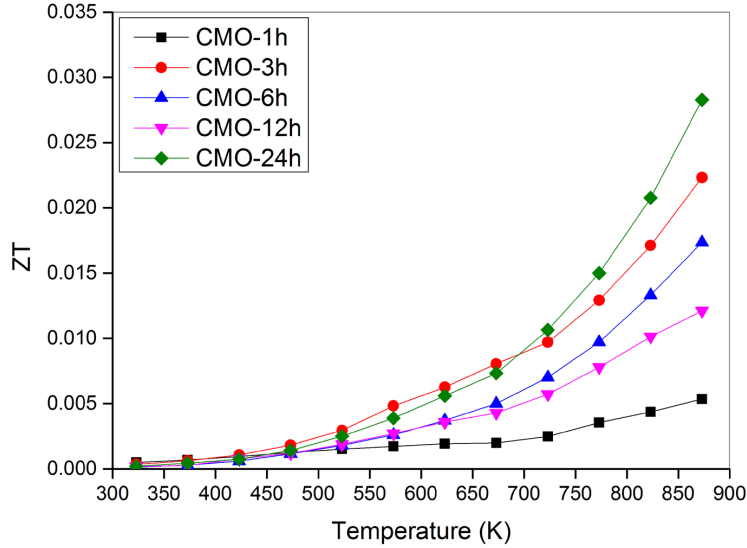


Figure 7. ZT values of the CMO ceramics.

by the model proposed for degenerate semiconductors⁶⁵, as expressed in Equation 4.

$$S = \left(\frac{8\pi^2 k_B^2}{3eh^2} mT \right) \left(\frac{\pi}{3n} \right)^{2/3} \quad (4)$$

where k_B is the Boltzmann constant and n and m^* refer to the carrier concentration and the effective mass of the carrier, respectively. Snyder and Toberer¹ and Li et al.⁶⁶ concluded that materials with low charge carrier concentration present as consequence high Seebeck coefficients values and low electrical conductivities, as also observed in this study. Srivastava et al.⁶⁷, observed in SrTiO₃ ceramics the reduction of the Seebeck coefficient and the increase in electrical conductivity with the increase of the sintering time. In the present study, this same behavior can be observed and attributed to the increase of the charge carriers, occasioned by the manganese valence change. The S values found in the literature for CMO ceramics are between $-180 \mu\text{V/K}$ and $-350 \mu\text{V/K}$ ^{13,32,68-70} for temperature range between 300 K and 900 K, which are in agreement with this study. CMO-1h ceramic presents higher Seebeck values at low temperatures and exceptionally low electrical conductivity, compared to the other ceramics. As discussed before, the low electrical conductivity indicates low charge carrier concentration in the ceramic, improving significantly Seebeck effect and increasing its values.

The Figure of Merit (ZT) values for the ceramics, calculated from Equation 1, are shown in Figure 7. The enhancement of ZT values is related to the increase of the sintering time. ZT values for CMO ceramics at 873 K are between 0.005 and 0.028 for CMO-1h and CMO-24h, respectively. In general, the increase in sintering time led to an improvement in ZT values in CMO ceramics. Increasing sintering time, the Seebeck coefficient value was changed by 38.5%, the electrical conductivity increased by 583.5% and the thermal conductivity was increased by 21.4%. Since the calculation of the ZT values depends directly

on these three parameters, the values were affected more significantly by the electrical conductivity in relation to the thermal conductivity and Seebeck coefficient values.

As discussed before, the ceramics produced with higher sintering time, own higher grain size and lower porosity than the other ceramics. In this case, these two effects increase both electrical and thermal conductivities. But the contribution to enhancing electrical conductivity was more pronounced than to enhance thermal conductivity, which leads to an increase of 5.6 times the ZT values of the ceramics sintered from 1 to 24 h.

4. Conclusions

From the production of polycrystalline ceramics of CaMnO₃ by solid-state reaction, the microstructural characteristics and thermoelectric properties were evaluated about different sintering times. In the process of obtaining the calcined powders the presence of a secondary phase, CaMn₂O₄, was detected, but for the sintered samples this secondary phase was no longer present. The increase of the sintering time in the ceramics promoted the increase in the average grain sizes, reaching values between 2.8 to 6.5 μm . Also, the increase of the sintering time directly increased the densification of the samples, as, the apparent densities directly varied between 83% and 99%. The thermal conductivity increased with the sintering time, reaching values between 4.0 and 5.0 W/mK at 873 K. The Seebeck coefficient values do not undergo significant changes in sintering times at higher temperatures, with values between -350 and $-200 \mu\text{V/K}$. The differentiation of the sintering times allows to conclude that long sintering times can enhance the thermoelectric properties of CMO ceramics, due to the reduction in electrical resistivity presented by these samples, which causes increases in the values of electrical conductivity, presenting values of 1748 S/m at 873 K for CMO ceramic sintered for 24 hours. The factor that most contributed to enhance the ZT 's values of the samples is the

electrical conductivity. At last, increasing time sintering drove to increase the grain size and reduce the porosity of the CaMnO_3 ceramics, features which were more clearly seen in the ceramic sintered for 24 hours. Based on these issues, thermal and electrical conductivity increased by 21.4% and 583.5%, respectively, but the Seebeck coefficient changed by 38.5%. Somehow, the conjunction of these parameters was favorable to obtain growing values of ZT, from 0.005 to 0.028 at 873 K, between 1 and 24 hours of sintering, which leads to an increase in the ZT values in 5.6 times.

5. Acknowledgments

This study was supported by CNPq (National Council for Scientific and Technological Development of Brazil) and CAPES. ANP (National Agency of Petroleum, Natural Gas and Biofuels of Brazil) and Shell of Brazil through the Clause Investment in Research, Development, and Innovation, contained in the contracts for Exploration, Development, and Production of Oil and Natural Gas also supported this study.

6. References

- Snyder GJ, Toberer ES. Complex thermoelectric materials. *Nat Publ Gr*. 2008;7:105-14.
- Ioffe AF, Stil'bans LS, Iordanishvili EK, Stavitskaya TS, Gelbtuch A, Vineyard G. Semiconductor thermoelements and thermoelectric cooling. *Phys Today*. 1959;12(5):42-42.
- Wang XW, Lee H, Lan YC, Zhu GH, Joshi G, Wang DZ, et al. Enhanced thermoelectric figure of merit in nanostructured n-type silicon germanium bulk alloy. *Appl Phys Lett*. 2008;93(193121):1-3.
- Fergus JW. Oxide materials for high temperature thermoelectric energy conversion. *J Eur Ceram Soc*. 2012;32:525-40. <http://dx.doi.org/10.1016/j.jeurceramsoc.2011.10.007>.
- dos Santos AM, Thomazini D, Gelfuso MV. Cold sintering and thermoelectric properties of $\text{Ca}_3\text{Co}_4\text{O}_9$ ceramics. *Ceram Int*. 2020;46: 14064–14070. doi:<https://doi.org/10.1016/j.ceramint.2020.02.206>.
- Bitner M, Helmich L, Nietschke F, Geppert B, Oeckler O, Feldhoff A. Porous $\text{Ca}_3\text{Co}_4\text{O}_9$ with enhanced thermoelectric properties derived from Sol-Gel synthesis. *J Eur Ceram Soc*. 2017;37:3909-15. <http://dx.doi.org/10.1016/j.jeurceramsoc.2017.04.059>.
- Ito M, Furumoto D. Microstructure and thermoelectric properties of $\text{Na}_x\text{Co}_2\text{O}_4/\text{Ag}$ composite synthesized by the polymerized complex method. *J Alloys Compd*. 2008;450:517-20.
- Bocher L, Aguirre MH, Logvinovich D, Shkabko A, Robert R, Trottmann M, et al. $\text{CaMn}_{1-x}\text{Nb}_x\text{O}_3$ ($x \leq 0.08$) perovskite-type phases as promising new high-temperature n-Type thermoelectric materials. *Inorg Chem*. 2008;47(18):8077-85.
- Thiel P, Eilertsen J, Populoh S, Saucke G, Döbeli M, Shkabko A, et al. Influence of tungsten substitution and oxygen deficiency on the thermoelectric properties of CaMnO_3 . *J Appl Phys*. 2013;114(243707):1-9.
- Lan J, Lin Y, Mei A, Nan C, Liu Y, Zhang B, et al. High-temperature electric properties of polycrystalline La-doped CaMnO_3 ceramics. *J Mater Sci Technol*. 2009;25(4):535-8.
- Singh SP, Kanas N, Desissa TD, Einarsrud MA, Norby T, Wiik K. Thermoelectric properties of non-stoichiometric $\text{CaMnO}_{3-\delta}$ composites formed by redox-activated exsolution. *J Eur Ceram Soc*. 2020;40:1344-51. <http://dx.doi.org/10.1016/j.jeurceramsoc.2019.11.027>.
- Wang Y, Sui Y, Wang X, Su W. Effects of substituting La^{3+} , Y^{3+} and Ce^{4+} for Ca^{2+} on the high temperature transport and thermoelectric properties of CaMnO_3 . *J Phys D Appl Phys*. 2009;42(055010):1-10.
- Kabir R, Zhang T, Donelson R, Wang D, Tian R, Tan TT, et al. Thermoelectric properties of Yb and Nb codoped CaMnO_3 . *Phys Status Solidi Appl Mater Sci*. 2014;211(5):1200-6.
- Kawakami H, Saito M, Takemoto H, Yamamura H, Isoda Y, Shinohara Y. Thermoelectric properties of perovskite-type oxide Ca-Mn-O system in relation to A-site vacancies. *Mater Trans* [serial on the Internet]. 2013 [cited 2020 Apr 23];54(9):1818-22. Available from: <http://www.scopus.com/inward/record.url?eid=2-s2.0-84883241248&partnerID=40&md5=3fe32a71724bdd952fb76af83b4d04de>
- Zhang F, Niu B, Zhang K, Zhang X, Lu Q, Zhang J. Effects of praseodymium doping on thermoelectric transport properties of CaMnO_3 compound system. *J Rare Earths*. 2013;31(9):885-90. [http://dx.doi.org/10.1016/S1002-0721\(12\)60374-3](http://dx.doi.org/10.1016/S1002-0721(12)60374-3).
- Thiel P, Populoh S, Yoon S, Saucke G, Rubenis K, Weidenkaff A. Charge-carrier hopping in highly conductive $\text{CaMn}_{1-x}\text{M}_x\text{O}_{3-\delta}$ Thermoelectrics. *J Phys Chem C*. 2015;119(38):21860-7.
- Feng X, Fan Y, Nomura N, Kikuchi K, Wang L, Jiang W, et al. Graphene promoted oxygen vacancies in perovskite for enhanced thermoelectric properties. *Carbon N Y*. 2017;112:169-76. <http://dx.doi.org/10.1016/j.carbon.2016.11.012>.
- Snyder GJ, Ursell TS. Thermoelectric efficiency and compatibility. *Phys Rev Lett*. 2003;91(14):148301/1-148301/4.
- Shin JF, Niu H, Alaria J, Claridge JB, Rosseinsky MJ. Substitution of Re^{7+} into CaMnO_3 : an efficient free electron generation dopant for tuning of thermoelectric properties. *Phys Chem Chem Phys*. 2017;19:30781-9.
- Paengson S, Pilasuta P, Singsook K, Namhongsa W, Impho W, Seetawan T. Improvement in thermoelectric properties of CaMnO_3 by Bi doping and hot pressing. *Mater Today Proc*. 2017;4:6289-95. <http://dx.doi.org/10.1016/j.matpr.2017.06.129>.
- Boldrin D, Boldrin P, Ruiz-Trejo E, Cohen LF. Recovery of the intrinsic thermoelectric properties of $\text{CaMn}_{0.98}\text{Nb}_{0.02}\text{O}_3$ in 2-terminal geometry using Ag infiltration. *Acta Mater*. 2017;133:68-72.
- Mishra A, Bhattacharjee S. Effect of A- or B-site doping of perovskite calcium manganite on structure, resistivity, and thermoelectric properties. *J Am Ceram Soc*. 2017;100(10):4945-53.
- Lan J, Lin YH, Fang H, Mei A, Nan CW, Liu Y, et al. High-temperature thermoelectric behaviors of fine-grained Gd-doped CaMnO_3 ceramics. *J Am Ceram Soc*. 2010;93(8):2121-4.
- Banerjee A, Pal S, Bhattacharya S, Chaudhuri BK, Yang HD. Particle size and magnetic field dependent resistivity and thermoelectric power of $\text{La}_{0.5}\text{Pb}_{0.5}\text{MnO}_3$ above and below metal-insulator transition. *J Appl Phys*. 2002;91(8):5125-34.
- Matos I, Sérgio S, Lopes ME, Nunes MR, Jorge MEM. Effect of the sintering temperature on the properties of nanocrystalline $\text{Ca}_{1-x}\text{Sm}_x\text{MnO}_3$ ($0 \leq x \leq 0.4$) powders. *J Alloys Compd*. 2011;509:9617-26.
- Zhang B, Chang A, Zhao Q, Ye H, Wu Y. Synthesis and thermoelectric properties of Yb-doped $\text{Ca}_{0.9x}\text{Yb}_x\text{La}_{0.1}\text{MnO}_3$ ceramics. *J Electron Mater*. 2014;43(11):4048-55.
- Schneider CA, Rasband WS, Eliceiri KW. NIH Image to ImageJ: 25 years of image analysis. *Nat Methods*. 2012;9(7):671-5.
- Klosek-Wawrzyn E, Malolepszy J, Murzyn P. Sintering behavior of kaolin with calcite. *Procedia Eng*. 2013;57:572-82.
- Zaki MI, Hasan MA, Pasupulety L, Kumari K. Thermochemistry of manganese oxides in reactive gas atmospheres: probing redox compositions in the decomposition course $\text{MnO}_2 \rightarrow \text{MnO}$. *Thermochim Acta*. 1997;303:171-81.
- Zaki M, Hasan M, Pasupulety L, Kumari K. Thermochemistry of manganese oxides in reactive gas atmospheres: probing catalytic MnOx compositions in the atmosphere of $\text{CO}+\text{O}_2$. *Thermochim Acta*. [serial on the Internet]. 1998 [cited 2020 Apr 23];311:97-103. Available from: <http://www.sciencedirect.com/science/article/pii/S0040603197004176>
- Mouyane M, Itaalit B, Bernard J, Houivet D, Noudem JG. Flash combustion synthesis of electron doped- CaMnO_3

- thermoelectric oxides. *Powder Technol.* 2014;264:71-7. <http://dx.doi.org/10.1016/j.powtec.2014.05.022>.
32. Kabir R, Tian R, Zhang T, Donelson R, Tan TT, Li S. Role of Bi doping in thermoelectric properties of CaMnO₃. *J Alloys Compd.* 2015;628:347-51.
 33. Schrade M, Kabir R, Li S, Norby T, Finstad TG. High temperature transport properties of thermoelectric CaMnO_{3-δ}: indication of strongly interacting small polarons. *J Appl Phys.* 2014;115(103705):103705-1-103705-7.
 34. Bocher L, Aguirre MH, Robert R, Logvinovich D, Bakardjieva S, Hejtmanek J, et al. High-temperature stability, structure and thermoelectric properties of CaMn_{1-x}Nb_xO₃ phases. *Acta Mater.* [serial on the Internet]. 2009;57(19):5667-80. Available from: <http://linkinghub.elsevier.com/retrieve/pii/S1359645409004972>
 35. Alfaruq DS, Otal EH, Aguirre MH, Populoh S, Weidenkaff A. Thermoelectric properties of CaMnO₃ films obtained by soft chemistry synthesis. *J Mater Res.* 2012;27(7):985-90.
 36. Mazur NM. Microstructural design of CaMnO₃ and its thermoelectric properties. Norwegian University of Science and Technology; 2015.
 37. Kabir R, Zhang T, Wang D, Donelson R, Tian R, Tan TT, et al. Improvement in the thermoelectric properties of CaMnO₃ perovskites by W doping. *J Mater Sci.* 2014;49:7522-8.
 38. Villars P, Cenzual K, editors. [Internet]. *CaMnO₃ crystal structure*. Berlin: Springer-Verlag Berlin Heidelberg & Material Phases Data System (MPDS), Japan: Switzerland & National Institute for Materials Science (NIMS); 2016 [cited 2020 Apr 23]. Available from: https://materials.springer.com/isp/crystallographic/docs/sd_1621032
 39. Ni C, Irvine JTS. Calcium manganite as oxygen electrode materials for reversible solid oxide fuel cell. *Faraday Discuss.* 2015;182:289-305.
 40. Melo Jorge ME, Correia dos Santos A, Nunes MR. Effects of synthesis method on stoichiometry, structure and electrical conductivity of CaMnO_{3-δ}. *Int J Inorg Mater.* [serial on the Internet]. 2001 [cited 2020 Apr 23];3:915-21. Available from: <http://www.sciencedirect.com/science/article/pii/S1466604901000885>
 41. Fu Y, Gu YJ, Chen YB, Liu HQ, Xu ZZ, Kong WL, et al. Effect of sintering time on Mn_{3d}/Mn_{4d} ratio and rate capability of spinel Li 1.02 Mn₂O₄. *Int J Electrochem Sci.* 2018;13(9):8817-26.
 42. Wang Y, Sui Y, Su W. High temperature thermoelectric characteristics of Ca_{0.9}R_{0.1}MnO₃ (R=La,Pr,...,Yb). *J Appl Phys.* 2008;104(9):093703.
 43. Almomani M, Shatnawi A. Effect of sintering time on the density, porosity content and microstructure effect of sintering time on the density, porosity content and microstructure of Copper – 1 wt. % silicon carbide composites. *Adv Mat Res.* 2015;1064:32-7.
 44. Zhang X, Chen G, Fu C, Cai W, Gao R, Wang F. Effects of sintering temperature and holding time on the microstructure and electric properties of Ba(Zr_{0.3}Ti_{0.7})O₃ ceramics. *Process Appl Ceram.* 2018;12(1):45-55.
 45. Bresch S, Mieller B, Delorme F, Chen C, Bektas M, Moos R, et al. Influence of reaction-sintering and calcination conditions on thermoelectric properties of sm-doped calcium manganate CaMnO₃. *J Ceram Sci Technol.* 2018;9:289-300.
 46. Wang Y, Sui Y, Fan H, Wang X, Su Y, Su W. High temperature thermoelectric response of electron-Doped CaMnO₃. *Chem Mater.* 2009;21(19):4653-60.
 47. Zhu Y-H, Su W-B, Liu J, Zhou Y-C, Li J, Zhang X, et al. Effects of dy and Yb co-doping on thermoelectric properties of CaMnO₃ ceramics. *Ceram Int.* 2015;41(1):1535-9.
 48. Franz R, Wiedemann G. Ueber die Wärme-Leitungsfähigkeit der Metalle. *Ann der Phys und Chemie.* 1853;165(8):497-531.
 49. Molinari M, Tompsett DA, Parker SC, Azough F, Freer R. Structural, electronic and thermoelectric behaviour of CaMnO₃ and CaMnO_(3-δ). *J Mater Chem A Mater Energy Sustain.* [serial on the Internet]. 2014 [cited 2020 Apr 23];2:14109-17. Available from: <http://xlink.rsc.org/?DOI=C4TA01514B>
 50. Kingery WD, Bowen HK, Uhlmann DR. *Introduction to ceramics*. 2nd ed. New York: Wiley Interscience; 1975. 1032 p.
 51. Wang N, Zhang K, Chai J, Xu T, Jia H, Chen J, et al. Folded thermoelectric cooling structure with Bi₂Te₃-based thin-film superlattices. *ECS J of Solid State Sci Technol.* 2018;7(8):136-41.
 52. Carter CB, Norton MG. *Ceramic materials - science and engineering*. New York: Springer; 2007. 716 p.
 53. Zhan B, Lan J, Liu Y, Lin Y, Shen Y, Nan C. High temperature thermoelectric properties of Dy-doped CaMnO₃ ceramics. *J Mater Sci Technol.* 2014;30(8):821-5. <http://dx.doi.org/10.1016/j.jmst.2014.01.002>.
 54. Mott NF, Davis EA. *Electronic processes in non-crystalline materials*. New York: Oxford University Press Inc.; 2012. 590 p.
 55. Tuller HL, Nowick AS. Small polaron electron transport in reduced CeO₂ single crystals. *J Phys Chem Solids.* 1977;38:859-67.
 56. Raffaele R, Anderson HU, Sparlin DM, Parris PE. Transport anomalies in the high-temperature hopping conductivity and thermopower of Sr-doped La(Cr,Mn)O₃. *Phys Rev B Condens Matter.* 1991;43(10):7991-9.
 57. Kannan R, Vanidha D, Arunkumar A. High temperature electrical transport properties of nanophase Ba_{1-x}Sb_xMnO₃. *Int J Eng Sci Technol.* 2013;5(6):1211-9.
 58. Leonidova EI, Leonidov IA, Patrakeev MV, Kozhevnikov VL. Oxygen non-stoichiometry, high-temperature properties, and phase diagram of CaMnO_{3-δ}. *J Solid State Electrochem.* [serial on the Internet]. 2011 [cited 2020 Apr 23];15:1071-5. Available from: <http://link.springer.com/10.1007/s10008-010-1288-1>
 59. Li Y, Hao S, Xia X, Xu J, Du X, Fang S, et al. Preparation, structure, and electrical properties of Ca_{1-x}Er_xMnO₃ powders. *J Electron Mater.* 2013;42(4):745-51.
 60. Hung LT, Van Nong N, Han L, Le Minh D, Borup KA, Iversen BB, et al. High-temperature thermoelectric properties of Ca_{0.9}Y_{0.1}Mn_{1-x}Fe_xO₃ (0 ≤ x ≤ 0.25). *J Mater Sci.* 2013;48:2817-22.
 61. Wang Y, Sui Y, Gong J, Yuan Z, Li C, Chen Q. Improved thermoelectric property of cation-substituted CaMnO₃. *Chin Phys B.* 2015;24(9):1-6.
 62. Kannan R, Vanidha D, Kumar AA, Tulasi KUR, Sivakumar R. Metal-insulator phase transition and structural stability in 'Sb' doped CaMnO₃ perovskite. *Int J Mater Sci Appl.* 2013;2:128-35.
 63. Seebeck TJ. *Magnetische Polarisation der Metalle und Erze durch Temperatur-Differenz (Magnetic polarization of metals and minerals by temperature differences). Abhandlungen der Königl. Akad. der Wissenschaften zu Berlin*. Berlin: Treatises of the Royal Academy of Sciences in Berlin; 1825. p. 265-373.
 64. Park JW, Kwak DH, Yoon SH, Choi SC. Thermoelectric properties of Bi, Nb co-substituted CaMnO₃ at high temperature. *J Alloys Compd.* 2009;487(1-2):550-5.
 65. Cutler M, Leavy JF, Fitzpatrick RL. Electronic transport in semimetallic cerium sulfide. *Phys Rev.* 1964;133(4A):A1143-52.
 66. Li C, Chen Q, Yan Y. Effects of Pr and Yb dual doping on the thermoelectric properties of CaMnO₃. *Materials (Basel).* 2018;11:1-13.
 67. Srivastava D, Norman C, Azough F, Schäfer MC, Guilmeau E, Kepaptsoglou D, et al. Tuning the thermoelectric properties of A-site deficient SrTiO₃ ceramics by vacancies and carrier concentration. *Phys Chem Chem Phys.* 2016;18:26475-86.
 68. Flahaut D, Funahashi R, Lee K, Ohta H, Koumoto K. Effect of the Yb substitutions on the thermoelectric properties of CaMnO₃. *Int Conf Thermoelectr ICT.* 2006:103-6.
 69. Huang XY, Miyazaki Y, Kajitani T. High temperature thermoelectric properties of Ca_{1-x}Bi_xMn_{1-y}V_yO_{3-δ} (0 ≤ x=y ≤ 0.08). *J Mater Chem C Mater Opt Electron Devices.* 2008;145:132-6.
 70. Flahaut D, Mihara T, Funahashi R, Nabeshima N, Lee K, Ohta H, et al. Thermoelectrical properties of A -site substituted Ca_{1-x}Re_xMnO₃ system. *J Appl Phys.* 2006;100:1-4.